Trends in Global Vegetative Drought From Long-Term Satellite Remote Sensing Data

Zhanya Xu, Leiyu Cao, Shaobo Zhong, Geng Liu, Yongsheng Yang, Shuang Zhu, Xiangang Luo, and Liping Di, *Senior Member, IEEE*

***Abstract*—in this article, the trends in global vegetative drought were investigated using MODIS- and AVHRR-based NDVI products. A set of selected methods were employed to perform trend analysis including trend test, trend location detection, and trend estimates. Accounting for the effect of the global geographical heterogeneity on trend analysis, the NDVI dataset was aggregated on designated divisions in view of latitude ranges and climate zones. From the results, it was concluded that: AVHRR has longer-term records that provide a critical historical perspective on vegetation activities necessary for global change research, and continuity and correctness is achievable from AVHRR VCI given the systematic offset between the NDVI values derived from the two sensors and the characteristics of the VCI algorithm. From a pixel level global trend analysis map, the proportion of pixels with rising trends is 54.7% in the world, 67.6% and 47.5% in the northern hemisphere and the southern hemisphere, respectively, which means there is an overall rising trends in the global VCI values, especially in the northern hemisphere. The North Temperate and the South Tropical have overall increases in the VCI values while all climate zones have overall increases in the VCI values. The piecewise trends basically adhere to the results of overall trend identification although there are some local variations. There are obvious rising trends during the latest years for all the climate zones. Dominant down trends were identified in A, B, Cw, Ds, and E while the piecewise trends for both Cs and Df are dominantly rising before 2000. An average of about four breakpoints were detected from both the climate zone- and latitude range-aggregated divisions Thus, the mean duration for a piecewise trend is 7–9 years.**

***Index Terms*—AVHRR, MODIS, trend analysis, vegetation condition index (VCI), vegetative drought.**

I. Introduction

DROUGHT is one of the worst natural disasters because it develops slowly and occurs in a large scope. It also causes other secondary disasters such as fires, diseases, and locust plagues, further aggravating the impact and consequences of disasters. Global food safety arising from drought-induced crop failure is one of the greatest concerns [1], [2]. Furthermore, drought is an important indicator for climate, environmental, or ecological changes. Frequent and prolonged periods of drought also cause adverse ecological and environmental impacts, such as shortage of water resources, increased desertification, frequent occurrence of dust storms, etc. In return, these large-scale effects may also thoroughly alter the evolution of drought and characteristics of vegetation response to drought.

With advances in international collaboration of meteorological observations and satellite remote sensing, the study of the long-term evolution of drought at global and regional scales has been one of the most popular topics in recent decades. Investigating global drought trends contributes to evaluation to the effect of global climate change and human activity and policy-making to sustainable development. To ecologists' interest, separating short-term weather signal from vegetation response to drought, long-term ecological system changes all over the world may be identified, which will provide substantial references for environmental and ecological solutions [3], [4]. As a way to investigate long-term evolution of drought, trend analysis on time series data have been widely performed from regional to global scales in terms of long-term meteorological records (e.g., precipitation and temperature) [5]–[8]. While meteorological drought represents deficit of water balance due to little precipitation or strong evapotranspiration, vegetative drought indicates plants' response to weather signals.

In remote sensing, NDVI is widely used for assessment of vegetation coverage and its growth vigor [9]. In fact, the drought depresses vegetation growth, which reduced NDVI. Many researchers and institutions pay attention to theories and applications of vegetative drought detection using remote sensing. In recent decades, a NDVI derived index: VCI has been used many times to detect and monitor agriculture droughts around the globe [10]–[14]. Many researchers found that vegetation state mainly depends on long-term ecological changes and short-term weather inputs, and weather signal in an NDVI value is weaker than the ecological one [15], [16]. In order to separate the short-term weather-related NDVI fluctuations from the long-term ecosystem changes, Kogan [10] proposed a AVHRR-based drought monitoring approach and provided new AVHRR-based vegetation condition index (VCI) that has shown to be useful for drought detection and tracking. Validations and some

Manuscript received November 25, 2019; revised January 19, 2020; accepted February 3, 2020. Date of publication February 10, 2020; date of current version March 2, 2020. The work of S. Zhong was supported by the Beijing Municipal Science and technology Project under Grant Z191100001419002. The work of S. Zhu was supported by the National Natural Science Foundation of China under Grant 51809242. *(Corresponding author: Shaobo Zhong.)*

Zhanya Xu, Leiyu Cao, Geng Liu, Shuang Zhu, and Xiangang Luo are with the School of Geography and Information Engineering, China University of Geosciences, Wuhan 430074, China (e-mail: xuzhanya@cug.edu.cn; caoleiyu@cug.edu.cn; liulaogeng@cug.edu.cn; zhushuang@cug.edu.cn; billlxg@126.com).

Shaobo Zhong is with the Beijing Research Center of Urban Systems Engineering, Beijing 100035, China (e-mail: zhongshaobo@gmail.com).

Yongsheng Yang is with the Department of Engineering Physics/Institute of Public Safety Research, Tsinghua University, Beijing 100084, China (e-mail: yangyongsheng036@163.com).

Liping Di is with the Center for Spatial Information Science and Systems, George Mason University, Fairfax, VA 22032 USA (e-mail: ldi@gmu.edu).

Digital Object Identifier 10.1109/JSTARS.2020.2972574

applications showed that the VCI has an excellent ability to detect drought and to measure time of its onset, intensity, duration, and impact on vegetation [17]–[23].

Similarly, MODIS-based VCI was calculated and applied to drought monitoring [23]. As a continuity with NOAA's AVHRR NDVI time series record for historical and climate applications, some researchers believe that MODIS is most likely to achieve the better results than AVHRR does according to theoretical analysis and experimental results [24]. Nonetheless, AVHRR has a temporal coverage of exceeding 30 years. Previous researches related to MODIS-based drought monitoring reported that MODIS-based VCI is also beneficial for vegetative drought identification [23], [25].

The satellite-based drought indicators are generally preferential for the study and application of agricultural drought on large-scale regions, since the advantages of the pixel-level data over meteorological data-based drought indices include the provision of spatial detail and the availability with low cost [17], [26]–[28]. With several decadal accumulations of remotely sensed data and products and advances in satellite-based vegetative drought detection methods, the identification of global characteristics of vegetative drought are feasible from those long-term historical inventory data. Nonetheless, no studies have been reported on global characteristics of vegetative drought based on long-term data.

In this article, our aim is to investigate the trends of global vegetative drought using both the original AVHRR- and MODIS-based NDVI products during 1981–2019. A set of selected methods were employed to perform trend analysis including trend test, trend location detection, and trend estimates. The information may provide analytical clues for earth's large-scale pattern identification, such as identification of phenological characteristics and ecological system changes.

II. Data and Method

A. Retrieving Vegetation Indices

Vegetation index data from AVHRR and MODIS were employed to explore trends of global vegetative drought. With the two separate sets of data, we are intended to make a comparison and consolidate our findings.

NOAA NESDIS STAR (Center for Satellite Applications and Research) produces and disseminates so-called smoothed normalized difference vegetation index (SMN) products based on the original NDVI calculated from the GAC data [29]–[31]. The SMN is produced by applying an empirical distribution function statistical technique and a digital smoothing filter to the original NDVI orderly [28], [29], [32], and provided with 4km/16km spatial and seven-day composite temporal resolutions. The quality assessment data are provided together with each period of the vegetation index data. A least significant bits method is used to mark the land cover type or data quality for each pixel.

The MODIS has been a new powerful sensor widely used in many domains since launched in 1999. The MODIS instruments onboard two polar orbit satellites: Aqua and Terra are identical. Two vegetation indices: NDVI and enhanced vegetation index (EVI) are derived from atmospherically-corrected reflectance in the red, near-infrared, and blue wavebands. They use a MODIS-specific compositing method based on product quality assurance metrics to remove low-quality pixels. From the remaining good quality values, a constrained view angle approach then selects a pixel to represent the compositing period (from the two highest NDVI values it selects the pixel that is closest-to-nadir). The MODIS vegetation index product MOD13C1 was selected to calculate VCI, which has a spatial resolution of 5 km and 16-day intervals. A smoothing process called lowess was executed to produce MODIS SMN referring to [23].

B. Determining Divisions

Two types of factors: world climate zone and latitude range, are jointly considered to divide the whole globe into different geographical divisions. The world climate zones were first defined and produced by Köppen and Geiger [33]. Key to calculate the climate formula of Köppen and Geiger is the main climates and subsequent precipitation conditions [34]. The Köppen and Geiger's classification is a hierarchical form and finally determined 32 lowest level classes based on those conditions. Considering the study scale, the finest 32 classes were aggregated into nine classes, i.e., equatorial climates (A), arid climates (B), warm temperate climate with dry summer (Cs), Warm temperate climate with dry winter (Cw), warm temperate climate, fully humid (Cf), snow climate with dry summer (Ds), snow climate with dry winter (Dw), snow climate, fully humid (Df), and polar climates (E). This treatment makes us be able to investigate the drought characteristics by different climate zones. At the same time, it avoids being trapped into too many details. The distribution of the new demarcated classes is shown as Fig. 1.

To investigate the association of vegetative drought with latitude range, the globe was also divided into six latitude ranges: north frigid (66.5–90 degrees), north temperate (23.5–66.5 N degrees), north tropical (0–23.5 N degrees), south tropical (0–23.5 S degrees), south temperate (23.5–66.5 S degrees), south frigid (66.5–90 S degrees).

Finally, trends of vegetative drought were evaluated in designated divisions with specific climates and latitude ranges.

C. Aggregating NDVI and Calculating VCI

The weekly/16-day NDVI data were aggregated with two sequential operations. First, the VCI values were averaged on the designated divisions in view of world climate zones and latitude ranges, and then the seven-day series of the division-averaged AVHRR NDVI were aggregated into 16-day series with the MVC algorithm [35]. Thus, the 16-day series of AVHRR and MODIS NDVI were obtained in the designated divisions. In the operations, mask operations was applied to exclude the pixels with nonvegetation types and bad or weak quality according to the quality assessment data.

Next, the absolute maximum and minimum of the aggregated NDVI were calculated for each division over n years (the whole study period) and used as the criteria to estimate the upper (favorable weather) and the lower (unfavorable weather) limits of the ecosystem resources. Further, for estimation of weather

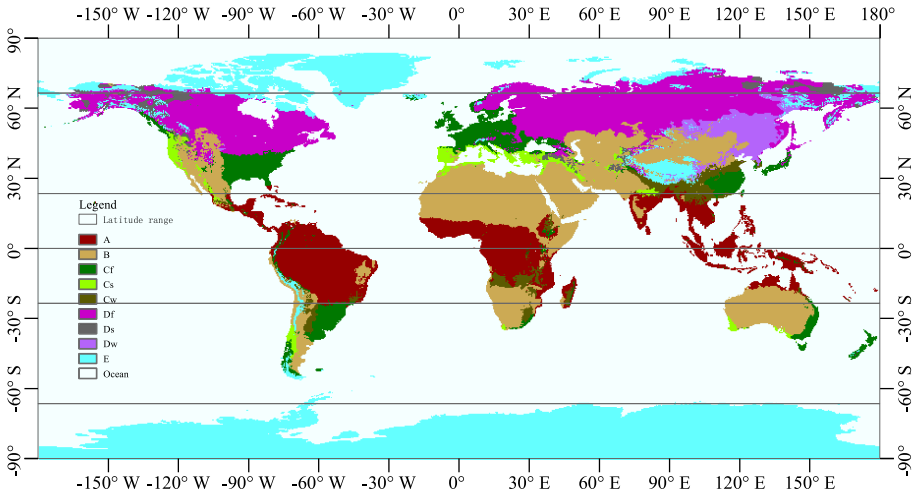

Fig. 1. Latitude ranges and world climate zones according to the reanalyzed Köppen–Geiger map [36].

impacts on vegetation condition, the NDVI values for a period were normalized relative to the absolute max/min intervals. Following this procedure, VCI in response to weather impacts can be written as follows [11]:

$$\mathrm{VCI} = 100 \times \frac{\mathrm{NDVI} - \mathrm{NDVI}_{\min}}{\mathrm{NDVI}_{\max} - \mathrm{NDVI}_{\min}} \tag{1}$$

where NDVI, $\mathrm{NDVI}_{\max}$, and $\mathrm{NDVI}_{\min}$ are the aggregated SMN, their absolute maximum and minimum over n years, respectively. The VCI approximate the weather component in NDVI. They fluctuate from 0 to 100, reflecting changes in vegetation conditions from extremely bad to optimal.

In the VCI formula above, the numerator indicates the meteorology and vegetation information of a specific period, and the denominator is the maximum differences between the best and worst conditions of vegetative growth which somewhat reflects the condition of the local vegetation [10], [15], [37]. The VCI contains both real-time and historical information of the NDVI.

D. Trend Detection and Estimates

1) Preprocessing of Series: According to [38], the existence of positive serial correlation in a time series increases the probability that some methods (e.g., Mann–Kendall test) detect a significant trend, i.e., serial correlation increases the type I error. Therefore, the series were also prewhitened to eliminate the effect of serial correlation before applying the Mann–Kendall test.

2) Trend Location Detection: In order to make trend analysis, the Mann–Kendall test with serial correlation was first used for trend identification [38]. Here, the Mann–Kendall test is performed on every divisions with data as an independent time-series test. The trend of each time series is recorded as z-score and p-value. The smaller the p-value is, the more statistically significant the trend is. The symbols associated with the z-score determine whether the trend is an increase in values (positive z-score) or a decrease (negative z-score). Then the sequential version of the Mann–Kendall test was used [39]–[43] to detect trend location in the VCI time series. This method is used to test a hypothesis about the beginning of the trend development within a sample [44]. The sequential version of the Mann–Kendall could be considered as an effective way of locating the beginning month(s) of a trend.

3) Trend Estimates: Considering that the least squares estimator for the coefficient β of a linear regression is vulnerable to gross errors and the associated confidence interval is sensitive to nonnormality of the parent distribution, Sen proposed a simple and robust (point as well as interval) estimator of β based on Kendall's rank correlation tau [45]. In this article, the Sen's method was used to estimate the slopes of trends.

III. Results

A. Consistency of VCI Series From MODIS and AVHRR

A total of 34 pairs of locations with complete valid values (no missing data) in MODIS- and AVHRR-derived VCI image series were selected and these locations are distributed in the global continents. As shown in Figs. 2, five of them were located in North America, five in South America, 15 in Africa, three in Asia, and six in Australia. The sample size for evaluation is larger than or comparable to several existing studies such as [46], [47] and these locations covers different latitude ranges, climate, land cover, terrain, etc., which is helpful for reducing the effect of sample bias on the evaluation results.

Fig. 3 shows the 16-day SMN series from MODIS and AVHRR datasets for the 34 selected locations. It can be seen that both instruments are able to feature the seasonal prosperity and recession of the vegetation overall. The similarity of the series looks fairly satisfactory except a systematic positive offset for MODIS in a visual inspection. AVHRR data are well connected to MODIS data in 2000 indicating that AVHRR observations can be extended with MODIS sensors after considering the systematic offset. This kind of data continuity is very important, which enables scientists to measure the impact of global environmental change on terrestrial ecosystems [46].

Fig. 4 shows the 16-day series of VCI values from MODIS and AVHRR for the selected 34 locations during 2000–2019.

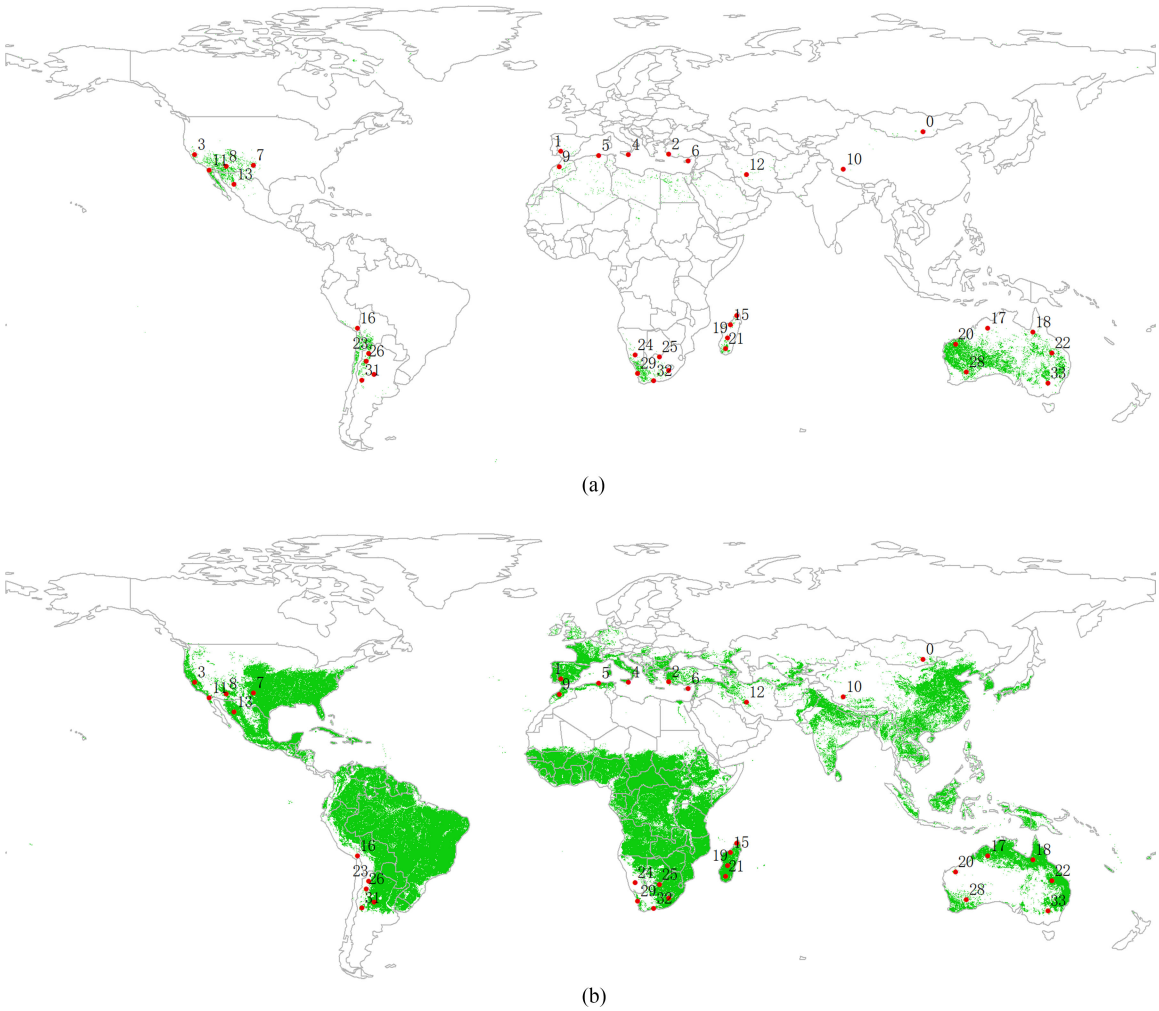

Fig. 2. Remaining pixels (green) having no missing values in the 16-day NDVI images (a) for MODIS and (b) for AVHRR. 34 locations as marked as red dots were selected to compare their corresponding series of VCI values between MODIS and AVHRR.

Overall, most of curve pairs show good consistency. From visually inspecting the corresponding curve pairs in Figs. 3 and 4, despite both show good similarity, we can find the patterns of differences between NDVI values from MODIS and AVHRR are quite different from those between VCI values from them. This inconformity comes from the nonlinearity of the algorithm transforming NDVI to VCI as (1).

On the correlations between MODIS- and AVHRR-derived VCI series, the column r of Table I shows the Pearson correlation coefficients and the column p-value shows the corresponding p-values. The root-mean-square error (RMSE) between the two sets of series for each location are displayed in the RMSE column of Table I. Almost all locations have an extremely significant level (p-value$<$0.001) from the p-value except location 16 (even so, the p-value of it is also less than 0.1). The smallest r is 0.102 (location 16), the biggest r is 0.968 (location 9), and the average r is 0.761, indicating strong correlations between two VCI series from MODIS and AVHRR, and from the RMSE, a relatively small bias can be seen. This means the similarity between two sets of VCI series is fairly good, and thus, either sensor-derived VCI can be used to detect vegetative drought in a sense of data applicability. Nonetheless, the dataset from AVHRR was selected to make analysis in view of its longer time span.

B. Overall Trends of VCI Values From AVHRR

A pixel level overall trend map of global drought and its corresponding p-value map were produced and shown in Fig. 5.

For each pixel location, a 16-day series was extracted from the AVHRR VCI dataset. Then, the Sen' method was applied to estimate the slopes of the overall trends of the series. Since the Sen's method can overcome some shortcomings of the least squares, the results were supposed to be more robust. From a visual inspection of the global trend map, positive trends are dominant in the northern hemisphere. Whereas, negative trends are more obvious in some areas of South America and Africa. The proportion of increasing trends is 54.7% in the world, which is 67.6% in the northern hemisphere and 47.5% in the southern hemisphere.

Sen's results of trend detection were given in Table II for the climate zone VCI series. All other climate zones have increasing trends with statistically significant levels except zone A, and E has the largest magnitude, followed by Dw, Cs, and Cf in turn.

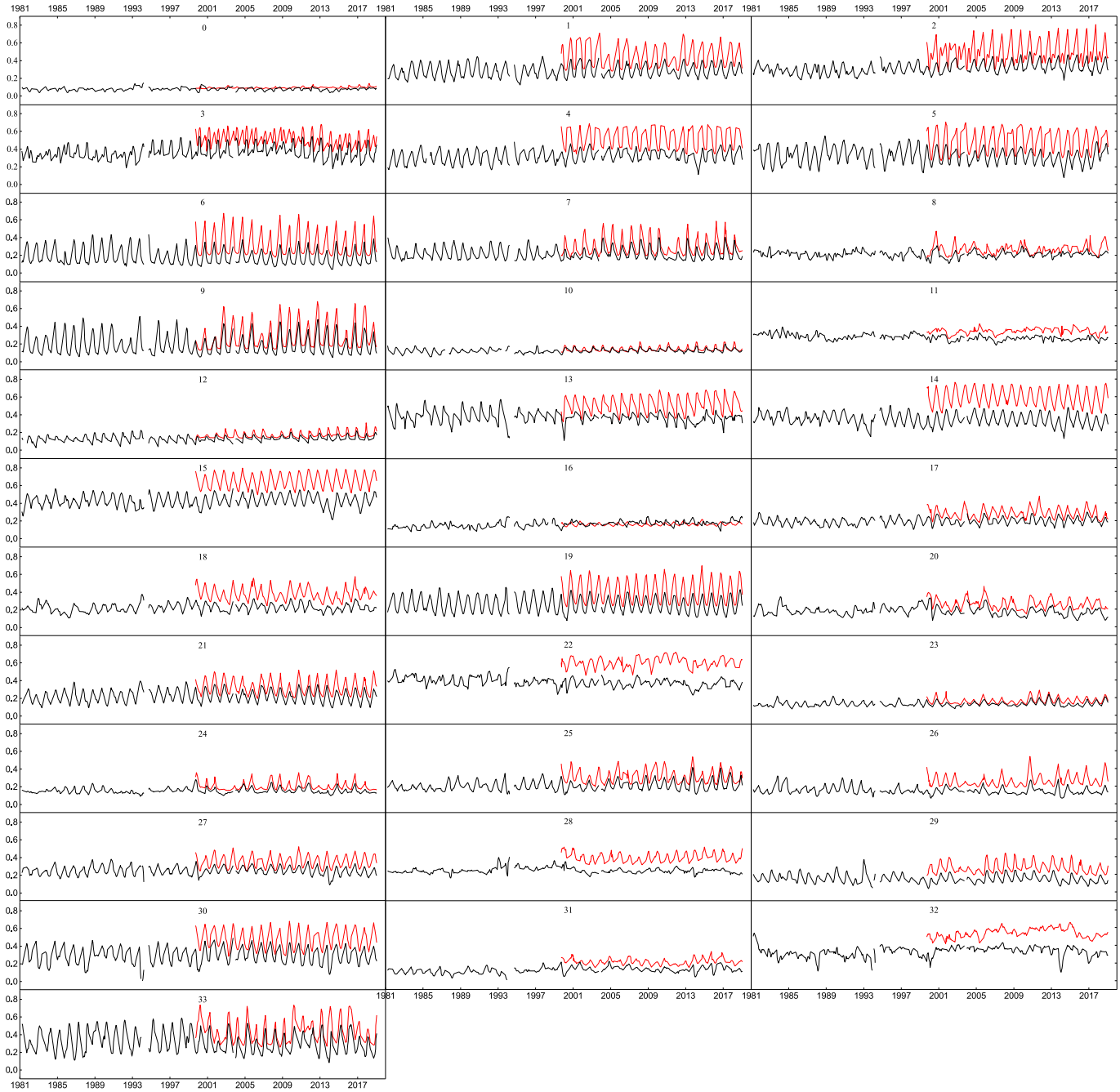

Fig. 3. SMN temporal profiles for the 34 selected locations. 16-day MODIS and AVHRR data are plotted. Before extracting the profiles, MODIS data were first aggregated to 16 km by calculating the average of all 5 km×5 km pixels in a 16 km×16 km window. The black lines show the time series of AVHRR 1981–2019 and the red lines show the time series of MODIS 2000–2019.

Table III presents results of trend test for latitude range VCI series. North temperate and south tropical have increasing trends with a statistically significant level.

C. Trends of Interannual Same Periods for VCI Values From AVHRR

Fig. 6 rendered the trends of inter-annual same periods for VCI values from AVHRR for climate zones (left panel) and latitude range divisions (right panel). The overall trends of every division test results were obtained with Mann–Kendall test considering serial correlation. The estimated slopes were plotted with heat map panels, where the slopes of the estimated trend lines were rendered with corresponding colors, specifically, green for positive trends and brown for negative trends. For the North Temperate, all 16-day periods-of-year during March–October have positive change trends in VCI values from 1981–2019, and from March to October, the trends gradually decreased. For the south tropical, there are generally slight trends of increase in VCI values. There are more periods with a decrease in VCI

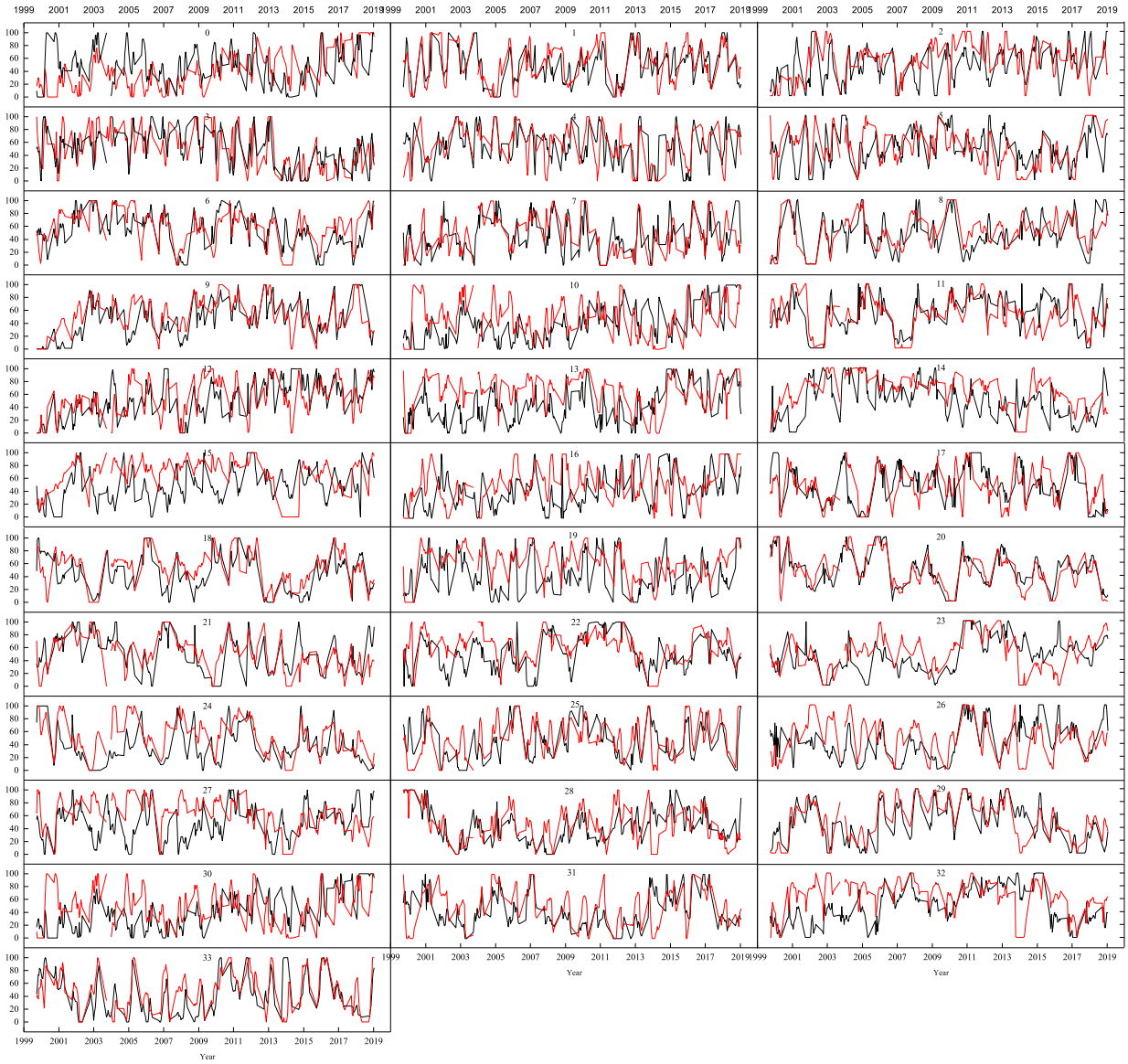

Fig. 4. VCI temporal profiles for the 34 selected locations. 16-day MODIS and AVHRR VCI data, which are derived from 16-day SMN in 2000–2009 as in Fig. 3, are plotted. The black lines show the time series of AVHRR and the red lines show the time series of MODIS.

values for the north tropical and south temperate. For the climate zones B, Cf, Cs, Df, Dw, and E, respectively, each period during March–October has positive trends. Among them, the positive trends for Cs, Dw, and E more obvious. For the climate zones A, Cw, and Ds, some periods showed negative trends and the strongest negative trends occurred in periods 161–177, 289, and 241, respectively.

D. Abrupt Changes of VCI Values From AVHRR

To detect breakpoints and evaluate trends, a *R* package "bfast" contributed by Verbesselt *et al.* was used [48], [49]. In the routine, the parameter h (minimal proportion of points during any two neighboring breakpoints) was set to 0.15, season (seasonal periodic function) was set to "harmonic."

Fig. 7 shows the 16-day series of latitude range aggregated VCI from AVHRR and the piecewise trend lines. The south frigid have too few VCI data to plot the curve and the north frigid has so many gaps at some locations of its curve, so we ignored the two latitude range divisions and finally only the breakpoint detection and trend analysis results for other four latitude range divisions were shown. From the curves of the VCI values, there are several common time points with small values that appear in 1992, 2000, and 2014 for different latitude range divisions. 4, 4, 5, and 4 breakpoints were identified from the north temperate to the south temperate, respectively. To ascertain the deviation from its normal level for a certain division, an anomaly index similar to [50] was calculated and superimposed. It is shown that the anomaly index curves basically has consistent changes with the VCI curves except for few points near zero. The piecewise trends were superimposed in the VCI curves as

TABLE I
PEARSON CORRELATION COEFFICIENT AND RMSE BETWEEN THE TWO SETS OF VCI SERIES FOR THE SELECTED 34 LOCATIONS

location	r	*p*-value	RMSE	location	r	*p*-value	RMSE
0	0.282	0.000	23.525	17	0.801	0.000	22.390
1	0.932	0.000	12.655	18	0.835	0.000	18.961
2	0.698	0.000	18.273	19	0.958	0.000	16.064
3	0.800	0.000	17.138	20	0.860	0.000	11.475
4	0.760	0.000	26.176	21	0.940	0.000	15.439
5	0.898	0.000	17.358	22	0.697	0.000	17.002
6	0.956	0.000	12.229	23	0.836	0.000	14.884
7	0.929	0.000	10.266	24	0.897	0.000	12.466
8	0.715	0.000	24.664	25	0.862	0.000	11.432
9	0.968	0.000	8.505	26	0.712	0.000	20.507
10	0.862	0.000	15.307	27	0.768	0.000	25.892
11	0.694	0.000	15.663	28	0.524	0.000	21.715
12	0.870	0.000	19.007	29	0.864	0.000	16.981
13	0.579	0.000	29.390	30	0.807	0.000	15.831
14	0.927	0.000	13.446	31	0.564	0.000	21.212
15	0.865	0.000	17.423	32	0.317	0.000	29.603
16	0.102	0.082	36.185	33	0.803	0.000	17.473

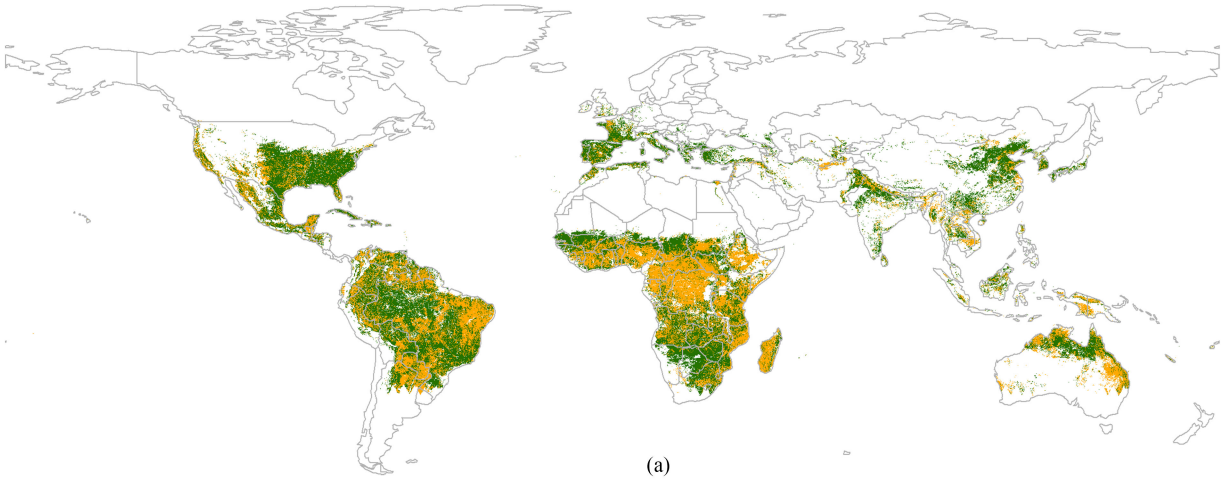

(a)

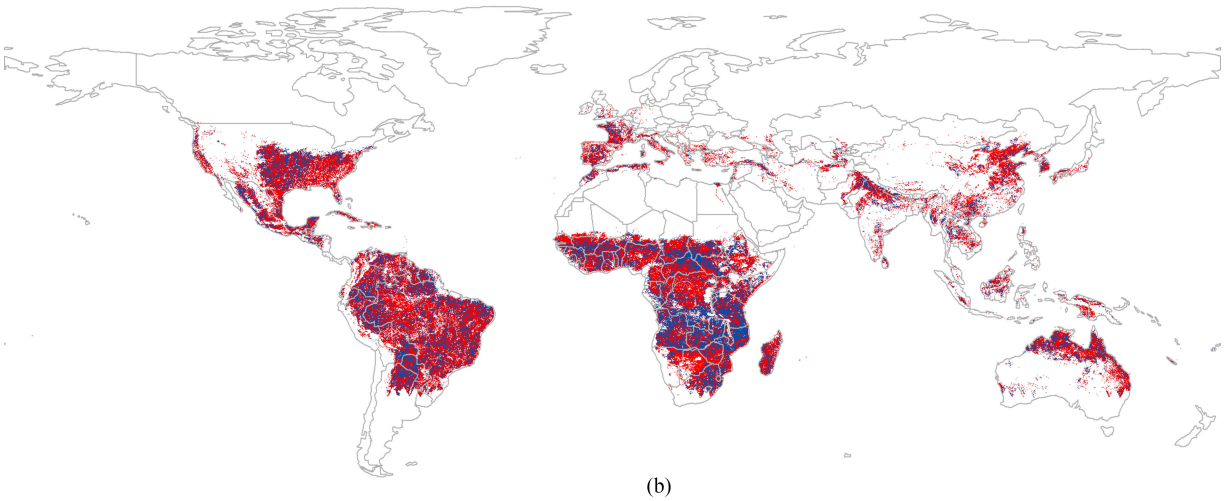

(b)

Fig. 5. (a) Pixel level overall trend map of global drought and (b) its corresponding p-value map from AVHRR VCI values. In (a), yellow and green denotes down trends and rising trends, respectively. In (b), red and blue denotes significant level (<0.1) and insignificant level (>0.1), respectively.

TABLE II
TREND DETECTION RESULTS FOR THE CLIMATE ZONE VCI SERIES

SEN	A	B	Cf	Cs	Cw	Df	Ds	Dw	E
trend	↑	↑	↑	↑	↑	↑	↑	↑	↑
b_sen	0.000	0.056	0.058	0.086	0.030	0.044	0.054	0.095	0.096
z	0.138	8.472	9.837	12.980	6.274	7.015	7.780	14.734	13.835
pval	0.891	0.000	0.000	0.000	0.000	0.000	0.000	0.000	0.000

TABLE III
RESULTS OF TREND TEST FOR LATITUDE RANGE VCI SERIES

SEN	North Frigid	North Temperate	North Tropical	South Tropical	South Temperate
trend	-	↑	↓	↑	↓
b_sen	-	0.090	-0.001	0.014	-0.004
z	-	13.690	-0.259	2.827	-0.735
pval	-	0.000	0.796	0.005	0.463

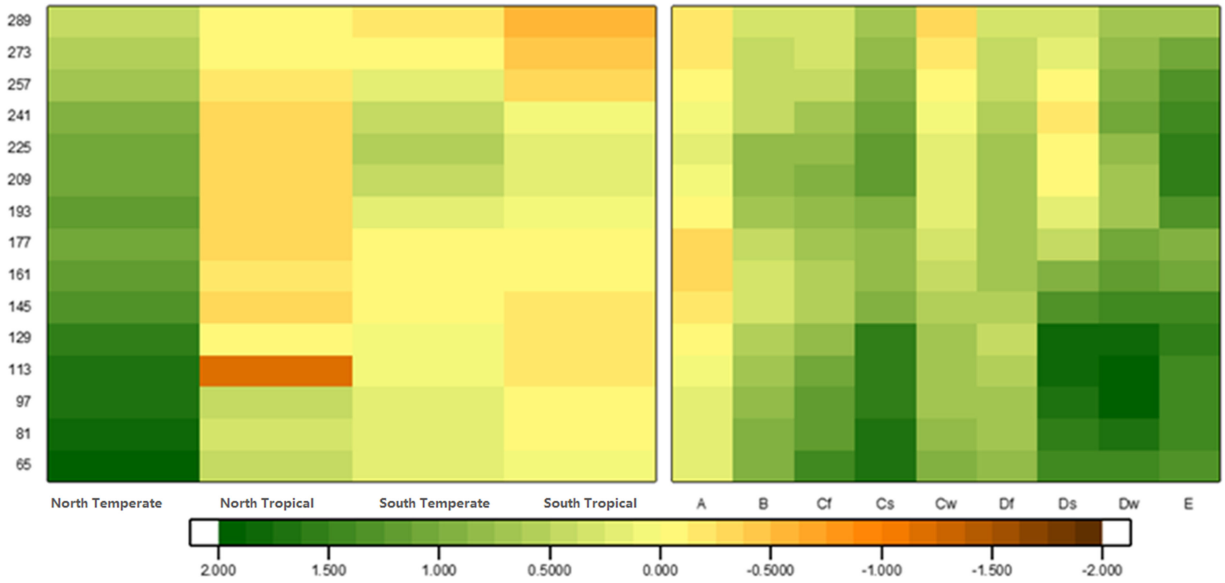

Fig. 6. Trend slopes for inter-annual same periods during March-October for VCI from AVHRR for different climate zones (left panel) and latitude range divisions (right panel).

shown in red lines in Fig. 7. Some abrupt change points can be seen from the superimposed plots. Generally, there are obvious rising trend during the latest years for all the four latitude range divisions. Before the end of the last century, the piecewise trends for the north temperate and the north tropical are all rising while those for the south tropical and south temperate are all down.

Fig. 8 shows the 16-day series of climate aggregated VCI from AVHRR and the piecewise trend lines. There are also several common small values appearing in 1992, 2000, and 2014, which is same as the latitude range aggregated series, indicating global strong vegetation stress in the years. The superimposed anomaly index curves basically have consistent changes with the VCI curves except for few points near zero. An average of about 4 (4, 4, 4, 3, 5, 3, 2, 4, and 3) breakpoints were detected from the climate zone A to the climate zone E. Several common breakpoints were identified from these series in periods 111, 154, 174, 196, 269, 290, 398, and 483, respectively. Some climate zones (e.g., A and Cw; Cf and E; and Cs and Df) have similar breakpoint locations in their overall series. There are obvious rising trends during the latest years for all the climate zones. Dominant down trends were identified in A, B, Cw, Ds, E while the piecewise trends for both Cs and Df are dominantly rising before 2000.

IV. DISCUSSION

From the comparison of MODIS NDVI and AVHRR NDVI, it is shown that MODIS NDVI has a positive offset from AVHRR NDVI at those selected locations. At this point, our findings

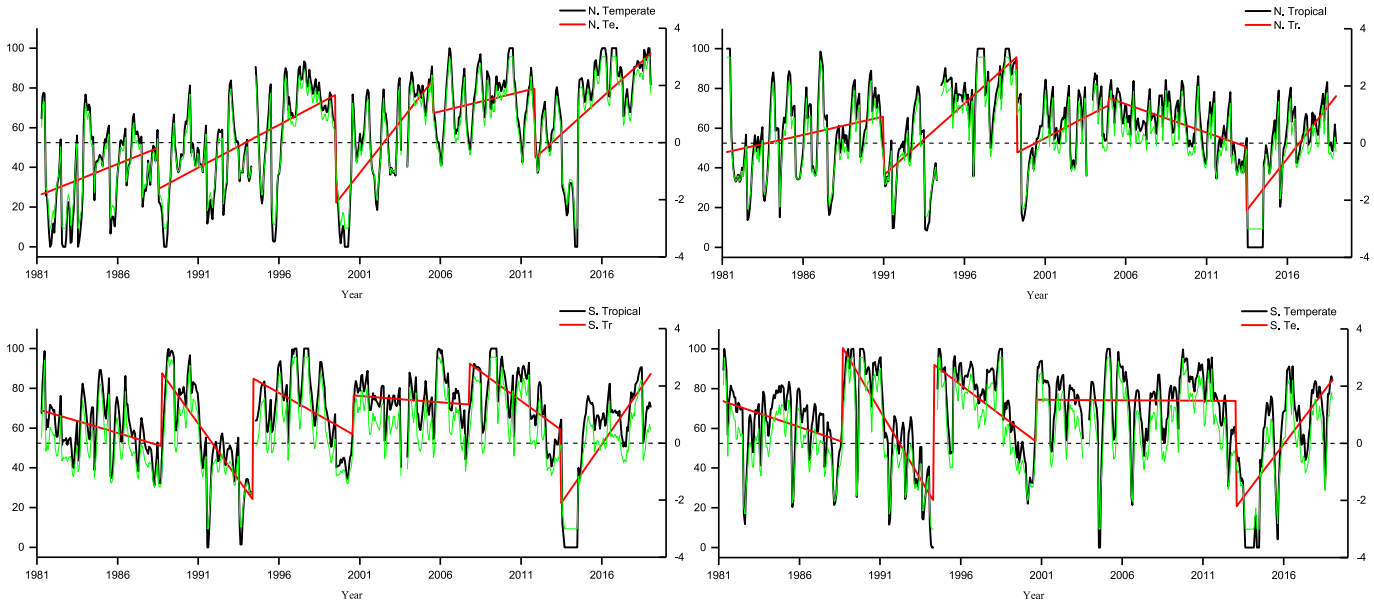

Fig. 7. Monthly series and breakpoint location and piecewise trends for north frigid, north temperate, north tropical, south tropical, and south temperate. An anomaly index was calculated and superimposed. The second *Y* axes are for the anomaly index.

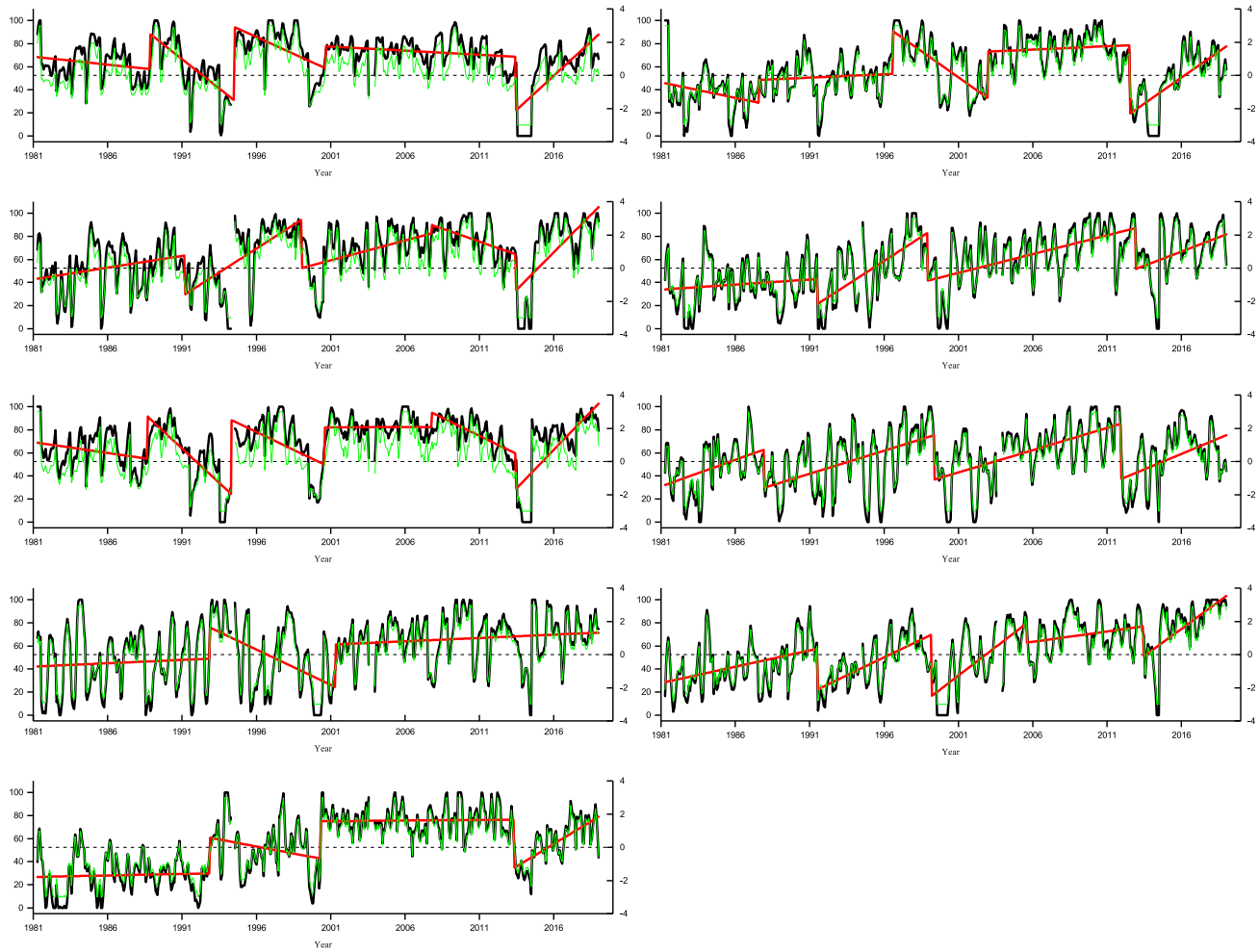

Fig. 8. 16-day climate zone aggregated VCI series from AVHRR and breakpoint location and piecewise trends for A, B, Cf, Cs, Cw, Df, Ds, Dw, and E. An anomaly index was calculated and superimposed. The second *Y* axes are for the anomaly index.

are consistent with previous studies [46], [51]. As a kind of more modern sensor, MODIS is considered to be able to provide higher quality. Nonetheless, AVHRR has longer-term record that provides a critical historical perspective on vegetation activities necessary for global change research. The results of comparison suggest that continuity is achievable given the systematic offset between the NDVI values derived from the two sensors and the characteristics of the VCI algorithm. In fact, after comparison between the two sensors, it can be seen that in general there is good consistency and similarity between them providing RMSE and correlations between some series of the two sensors from some selected locations distributed all over the globe. With regard to the overall trends, the north temperate and the south tropical have overall increases and the north tropical and south temperate have overall decreases in the VCI values. Some recent studies show the north part of south hemisphere is greening [52], which is a potential explanation for the increase in VCI in the north temperate. However, while examining the overall trends in climate zones, all climate zones have overall increases in the VCI values. This can be figured out jointly observing the coverage of these climates and reviewing the results of trend detection for latitude range divisions. The climate zones span different latitude range divisions including the north temperate and the south tropical that have significant rising trends in the aggregated VCI values and the two latitude range divisions take dominant roles over the other two latitude range divisions. From the trends of inter-annual same periods, the North Temperate has significant rising trends for all periods-of-year during March–October, which further revealed the greening findings and this trend spans the whole growth seasons of crops. Some researchers consider the global warming is one of the potential drivers for this findings [52]. In fact, many factors may make contribution to it such as crop rotation, irrigation patterns, urbanization, and disasters other than drought (e.g., flooding and biological infestation) [28]. These natural and social drivers may be investigated in global environmental and ecological research.

The results of breakpoint detection showed that some abrupt changes exist in the designated divisions including latitude range divisions and climate zones. The piecewise trends basically adhere to the results of overall trend identification although there are some local variations. The mean duration for a piecewise trend is 7–9 years. We think it is not accidental, but may be caused by the global El Nino and La Nina phenomena. For examples, some investigations at global and regional scales have presented clues and evidences of significant relationship between drought and global-scale climate change like El Nino [53]–[57].

In this article, designated divisions were obtained according to latitude ranges and climate zones, which mainly considers the two main factors affecting vegetative response to drought: temperature and precipitation. However, to explore the vegetative drought evolution dynamics in more details, more factors (e.g., terrain, vegetation type) should be taken into consideration. Therefore, in the follow-up research, Interest will focus on the underlying dominant drivers for the trends and variability of global vegetative drought, which include natural and man-made ones. For example, man activities such as agricultural manufacturing, artificial forest cultivation, water conservancy project contribute much to vegetation state conditions. In these cases, remote sensing monitoring of vegetative drought will fail to indicate the real drought conditions. Methods coupling remote sensing and meteorological observations will be necessary for better monitoring and forecast of drought.

V. Conclusion

At the global scale and using remote sensing, we first investigated trends in global vegetative drought. The long-term remotely sensed data from AVHRR (from 1981 to 2019) were used to investigate the global trend of vegetative drought. Nonetheless, as a newer sensor, MODIS is thought of as advanced and better. We compared the consistency of MODIS NDVI/VCI and AVHRR NDVI/VCI according to their overlapping period, which justifies the applicability of AVHRR NDVI/VCI for long-term vegetative drought investigation. As a result, AVHRR-derived VCI data were used to analyze the trend characteristics of global vegetative drought. In addition to the overall trend test, the trend locations and the corresponding piecewise slopes were also detected and estimated. Considering periodicity and serial correlation, the inter-annual series are also explored separately.

The methods used in this article are sound to detect trend locations and estimate trend slopes. In addition, accounting for the effect of the global geographical heterogeneity on trend analysis, the NDVI dataset was aggregated on designated divisions in view of latitude ranges and climate zones. This enables us to examine area-specific trend characteristics of vegetative drought.

The results of breakpoint location detection and trend analysis are reliable depending on the sound methods and with the comparison between our findings and some researchers' outcome in this field. From the results, we concluded that: there is an overall rising trends in the global VCI values. The north temperate and the south tropical have overall increases in the VCI values while all climate zones have overall increases in the VCI values. The piecewise trends basically adhere to the results of overall trend identification although there are some local variations. There are obvious rising trends during the latest years for all the climate zones. Dominant down trends were identified in A, B, Cw, Ds, E while the piecewise trends for both Cs and Df are dominantly rising before 2000. An average of about four breakpoints were detected from both the climate zone- and latitude range-aggregated divisions. Thus, the mean duration for a piecewise trend is 7–9 years.

Acknowledgment

The authors would like to thank the anonymous reviewers for their work and valuable suggestions. L. Di and S. Zhong principally conceived the idea for this study. L. Cao, G. Liu, and Y. Yang were engaged in setting up and completing experiments in the charge of Z. Xu. S. Zhu and X. Luo participated in experimental guidance and discussion. S. Zhong wrote the initial

draft of this article and responded the reviewers' comments. The authors declare no conflict of interest.

REFERENCES

[1] J. Schmidhuber and F. N. Tubiello, "Global food security under climate change," *Proc. Nat. Acad. Sci.*, vol. 104, no. 50, pp. 19703–19708, 2007.

[2] H. C. J. Godfray *et al.*, "Food security: The challenge of feeding 9 billion people," *Science*, vol. 327, no. 5967, pp. 812–818, 2010.

[3] X. H. Xu, Z. Q. Lv, X. Y. Zhou, and N. Jiang, "Drought prediction and sustainable development of the ecological environment," *Environ. Sci. Pollut. Res.*, vol. 24, pp. 26974–26982, 2017.

[4] T. E. Olagunju, "Drought, desertification and the Nigerian environment: A review," *J. Ecol. Natural Environ.*, vol. 7, no. 7, pp. 196–209, 2015.

[5] A. Dai, "Increasing drought under global warming in observations and models," *Nature Climate Change*, vol. 3, no. 1, pp. 52–58, 2013.

[6] E. J. Burke, S. J. Brown, and N. Christidis, "Modeling the recent evolution of global drought and projections for the twenty-first century with the Hadley Centre climate model," *J. Hydrometeorol.*, vol. 7, no. 5, pp. 1113–1125, 2006.

[7] K. M. Andreadis and D. P. Lettenmaier, "Trends in 20th century drought over the continental United States," *Geophys. Res. Lett.*, vol. 33, no. 10, 2006. doi: 10.1029/2006GL025711.

[8] J. Sheffield, E. F. Wood, and M. L. Roderick, "Little change in global drought over the past 60 years," *Nature*, vol. 491, no. 7424, pp. 435–438, 2012.

[9] C. J. Tucker and B. J. Choudhury, "Satellite remote sensing of drought conditions," *Remote Sens. Environ.*, vol. 23, no. 2, pp. 243–251, 1987.

[10] F. Kogan, "Application of vegetation index and brightness temperature for drought detection," *Adv. Space Res.*, vol. 15, no. 11, pp. 91–100, 1995.

[11] F. N. Kogan, "Global drought watch from space," *Bull. Amer. Meteorol. Soc.*, vol. 78, no. 4, pp. 621–636, 1997.

[12] F. Kogan, "World droughts in the new millennium from AVHRR-based vegetation health indices," *Eos, Trans. Amer. Geophys. Union*, vol. 83, no. 48, pp. 557–563, 2002.

[13] F. Kogan, R. Stark, A. Gitelson, L. Jargalsaikhan, C. Dugrajav, and S. Tsooj, "Derivation of pasture biomass in Mongolia from AVHRR-based vegetation health indices," *Int. J. Remote Sens.*, vol. 25, no. 14, pp. 2889–2896, 2004.

[14] C. Bhuiyan, R. Singh, and F. Kogan, "Monitoring drought dynamics in the Aravalli region (India) using different indices based on ground and remote sensing data," *Int. J. Appl. Earth Observ. Geoinf.*, vol. 8, no. 4, pp. 289–302, 2006.

[15] F. Kogan, "Remote sensing of weather impacts on vegetation in non-homogeneous areas," *Int. J. Remote Sens.*, vol. 11, no. 8, pp. 1405–1419, 1990.

[16] F. N. Kogan, "Vegetation index for areal analysis of crop conditions," in *Proc. 18th Conf. Agricultural Forest Meteorol.*, AMS W. Lafayette, 1987, pp. 103–106.

[17] A. Ahmadalipour, H. Moradkhani, H. Yan, and M. Zarekarizi, "Remote sensing of drought: vegetation, soil moisture, and data assimilation," in *Remote Sensing of Hydrological Extremes*, Berlin, Germany: Springer, 2017, pp. 121–149.

[18] R. P. Singh, S. Roy, and F. Kogan, "Vegetation and temperature condition indices from NOAA AVHRR data for drought monitoring over India," *Int. J. Remote Sens.*, vol. 24, no. 22, pp. 4393–4402, 2003.

[19] C. Domenikiotis, M. Spiliotopoulos, E. Tsiros, and N. Dalezios, "Early cotton yield assessment by the use of the NOAA/AVHRR derived vegetation condition index (VCI) in Greece," *Int. J. Remote Sens.*, vol. 25, no. 14, pp. 2807–2819, 2004.

[20] E. Tsiros, C. Domenikiotis, M. Spiliotopoulos, and N. Dalezios, "Use of NOAA/AVHRR-based vegetation condition index (VCI) and temperature condition index (TCI) for drought monitoring in Thessaly, Greece," in *Proc. EWRA Symp. Water Resour. Manage., Risks Challenges 21st century*, Izmir, Turkey, 2004, pp. 2–4.

[21] S. M. Quiring and S. Ganesh, "Evaluating the utility of the Vegetation Condition Index (VCI) for monitoring meteorological drought in Texas," *Agricultural Forest Meteorol.*, vol. 150, no. 3, pp. 330–339, 2010.

[22] D. Dutta, A. Kundu, N. Patel, S. Saha, and A. Siddiqui, "Assessment of agricultural drought in Rajasthan (India) using remote sensing derived vegetation condition index (VCI) and standardized precipitation index (SPI)," *Egyptian J. Remote Sens. Space Sci.*, vol. 18, no. 1, pp. 53–63, 2015.

[23] F. Zambrano, M. Lillo-Saavedra, K. Verbist, and O. Lagos, "Sixteen years of agricultural drought assessment of the biobío region in Chile using a 250 m resolution vegetation condition index (VCI)," *Remote Sens.*, vol. 8, no. 6, 2016.

[24] P. Toukiloglou, "Comparison of AVHRR, MODIS and VEGETATION for land cover mapping and drought monitoring at 1 km spatial resolution, Ph.D. dissertation, Dept. Natural Resour. Integr. Earth Syst. Sci. Inst., School Appl. Sci., Cranfield University, 2007.

[25] J. Zhang, Q. Mu, and J. Huang, "Assessing the remotely sensed Drought Severity Index for agricultural drought monitoring and impact analysis in North China," *Ecolog. Indicators*, vol. 63, pp. 296–309, 2016.

[26] A. AghaKouchak *et al.*, "Remote sensing of drought: Progress, challenges and opportunities," *Rev. Geophys.*, vol. 53, no. 2, pp. 452–480, 2015.

[27] S. Zhong, Z. Xu, Z. Sun, E. Yu, L. Guo, and L. Di, "Global vegetative drought trend and variability analysis from long-term remotely sensed data," in *Proc. IEEE 8th Int. Conf. Agro-Geoinform.*, 2019, pp. 1–6.

[28] S. Zhong, L. Di, Z. Sun, Z. Xu, and L. Guo, "Investigating the long-term spatial and temporal characteristics of vegetative drought in the contiguous United States," *IEEE J. Sel. Topics Appl. Earth Observ. Remote Sens.*, vol. 12, no. 3, pp. 836–848, Mar. 2019.

[29] F. Kogan, W. Guo, and A. Jelenak, "Global vegetation health: Long-term data records," in *Use of Satellite and In-Situ Data to Improve Sustainability*, Berlin, Germany: Springer, 2011, pp. 247–255.

[30] W. Guo, AVHRR vegetation health product (AVHRR-VHP) user guide, 2013.

[31] F. Kogan and J. Sullivan, "Development of global drought-watch system using NOAA/AVHRR data," *Adv. Space Res.*, vol. 13, no. 5, pp. 219–222, 1993.

[32] M. Ahmad, C. Sinclair, and B. Spurr, "Assessment of flood frequency models using empirical distribution function statistics," *Water Resour. Res.*, vol. 24, no. 8, pp. 1323–1328, 1988.

[33] M. C. Peel, B. L. Finlayson, and T. A. McMahon, "Updated world map of the Köppen-Geiger climate classification," *Hydrol. Earth Syst. Sci. Discuss.*, vol. 4, no. 2, pp. 439–473, 2007.

[34] W. Köppen, "Klassifikation der Klimate nach Temperatur, Niederschlag und Jahresablauf," *Petermanns Geogr. Mitt.*, vol. 64, pp. 193–203, 1918.

[35] B. N. Holben, "Characteristics of maximum-value composite images from temporal AVHRR data," *Int. J. Remote Sens.*, vol. 7, no. 11, pp. 1417–1434, 1986.

[36] M. Kottek, J. Grieser, C. Beck, B. Rudolf, and F. Rubel, "World map of the Köppen-Geiger climate classification updated," *Meteorol. Zeitschrift*, vol. 15, no. 3, pp. 259–263, 2006.

[37] F. N. Kogan, "Droughts of the late 1980 s in the United States as derived from NOAA polar-orbiting satellite data," *Bull. Amer. Meteorol. Soc.*, vol. 76, no. 5, pp. 655–668, 1995.

[38] A. Kulkarni and H. von Storch, "Monte Carlo experiments on the effect of serial correlation on the Mann-Kendall test of trend," *Meteorol. Zeitschrift*, vol. 4, no. 2, pp. 82–85, 1995.

[39] Y. Yang and F. Tian, "Abrupt change of runoff and its major driving factors in Haihe River Catchment, China," *J. Hydrol.*, vol. 374, no. 3-4, pp. 373–383, 2009.

[40] T. Partal and E. Kahya, "Trend analysis in Turkish precipitation data," *Hydrolog. Process.*, vol. 20, no. 9, pp. 2011–2026, 2006.

[41] M. Karaca, M. Tayanç, and H. n. Toros, "Effects of urbanization on climate of Istanbul and Ankara," *Atmos. Environ.*, vol. 29, no. 23, pp. 3411–3421, 1995.

[42] M. Kadioglu, "Trends in surface air temperature data over Turkey," *Int. J. Climatol.*, vol. 17, no. 5, pp. 511–520, 1997.

[43] F.-W. Gerstengarbe and P. C. Werner, "Estimation of the beginning and end of recurrent events within a climate regime," *Climate Res.*, vol. 11, no. 2, pp. 97–107, 1999.

[44] D. Karpouzos, S. Kavalieratou, and C. Babajimopoulos, "Trend analysis of precipitation data in Pieria Region (Greece)," *Eur. Water*, vol. 30, pp. 31–40, 2010.

[45] P. K. Sen, "Estimates of the regression coefficient based on Kendall's tau," *J. Amer. Statist. Assoc.*, vol. 63, no. 324, pp. 1379–1389, 1968.

[46] M. E. Brown, J. E. Pinzón, K. Didan, J. T. Morisette, and C. J. Tucker, "Evaluation of the consistency of long-term NDVI time series derived from AVHRR, SPOT-vegetation, SeaWiFS, MODIS, and Landsat ETM+ sensors," *IEEE Trans. Geosci. Remote Sens.*, vol. 44, no. 7, pp. 1787–1793, Jul. 2006.

[47] F. Tian, R. Fensholt, J. Verbesselt, K. Grogan, S. Horion, and Y. Wang, "Evaluating temporal consistency of long-term global NDVI datasets for trend analysis," *Remote Sens. Environ.*, vol. 163, pp. 326–340, 2015.

[48] J. Verbesselt, R. Hyndman, A. Zeileis, and D. Culvenor, "Phenological change detection while accounting for abrupt and gradual trends in satellite image time series," *Remote Sens. Environ.*, vol. 114, no. 12, pp. 2970–2980, 2010.
[49] J. Verbesselt, R. Hyndman, G. Newnham, and D. Culvenor, "Detecting trend and seasonal changes in satellite image time series," *Remote Sens. Environ.*, vol. 114, no. 1, pp. 106–115, 2010.
[50] V. Moron, "Guinean and Sahelian rainfall anomaly indices at annual and monthly scales (1933–1990)," *Int. J. Climatol.*, vol. 14, no. 3, pp. 325–341, 1994.
[51] L. Liu, Y. Liang, H. Ma, and J. Huang, "Relationship research between MODIS-NDVI and AVHRR-NDVI," *Geomatics Inf. Sci. Wuhan Uni.*, vol. 29, no. 4, pp. 307–310, 2004.
[52] Z. Zhu *et al.*, Greening of the earth and its drivers, 2016.
[53] D. Zopf, K. Short, and R. Yang Kuo, "Historical trends and statistics of the Southern Oscillation, El Niño and Indonesian droughts," *Fisheries Bull.*, vol. 76, pp. 663–678, 1978.
[54] M. C. Thomson, K. Abayomi, A. Barnston, M. Levy, and M. Dilley, "El Nino and drought in Southern Africa," *Lancet*, vol. 361, no. 9355, pp. 437–438, 2003.
[55] F. H. S. Chiew, T. C. Piechota, J. A. Dracup, and T. A. McMahon, "El Nino/Southern Oscillation and Australian rainfall, streamflow and drought: Links and potential for forecasting," *J. Hydrol.*, vol. 204, no. 1-4, pp. 138–149, 1998.
[56] T. C. Piechota and J. A. Dracup, "Drought and regional hydrologic variation in the United States: Associations with the El Nino Southern Oscillation," *Water Resour. Res.*, vol. 32, no. 5, pp. 1359–1374, 1996.
[57] C. A. D. S. Coelho and L. Goddard, "El Nino-induced tropical droughts in climate change projections," vol. 22, no. 23, pp. 6456–6476, 2009.

Zhanya Xu received the Ph.D. degree from the China University of Geosciences, Wuhan, China, in 2010.

He is currently a Lecturer with the School of Geography and Information Engineering, China University of Geosciences. He is a Member of the China Computer Federation. He has authored or coauthored more than 20 papers in journals and conferences. His research areas include spatial information services, big data processing, and intelligent computing.

Leiyu Cao received the graduate degree from Huazhong Agricultural University, Wuhan, China, in 2014. He is currently working toward the master's degree at China University of Geosciences, Wuhan, China.

His research interest includes surveying engineering, with a focus on cartography and geographic information engineering.

Shaobo Zhong is born in Hubei, China, in 1978. He received the Ph.D. degree in cartography and GIS from Institute of Remote Sensing Applications, Chinese Academy of Sciences, Wuhan, China, in 2006.

He was an Educator and a Researcher with Tsinghua University, Beijing, China, until the end of 2018. He is currently an Associate Researcher with Beijing Researcher Center of Urban Systems Engineering, Beijing, China. He has authored or coauthored more than 100 papers. His research interests include geoinformation for disasters, resilient and risk assessment of disastrous meteorological events, spatial big data and machine learning for spatial and temporal problem solving, particularly in safety operations of smart city.

Geng Liu is currently working toward the M.S. degree at the School of Geography and Information Engineering, China University of Geosciences, Wuhan, China.

His research areas include spatial information services, remote sensing data analysis, and intelligent computing.

Yongsheng yang is currently working toward the Ph.D. degree at Tsinghua University, Beijing, China.

His research interest includes risk assessment of public safety.

Shuang Zhu received the Ph.D. degree from the Huazhong University of Science and Technology, Wuhan, China, in 2017.

She is currently a researcher with the School of Geography and Information Engineering, China University of Geosciences, Wuhan, China. Her research interests include hydrology modeling, forecasting and analysis, extreme meteorological, and hydrological events.

Xiangang Luo received the Ph.D. degree from the China University of Geosciences, Wuhan, China, in 2010.

He is currently an Associate Professor with the School of Geography and Information Engineering, China University of Geosciences. He has authored or coauthored more than 20 papers in journals and conferences. His research interests include big data analysis, environmental monitoring, and spatial information services..

Liping Di (Senior Member, IEEE) received the Ph.D. degree in remote sensing/GIS (geography) from the University of Nebraska–Lincoln, Lincoln, NE, USA, in 1991.

He is the Founding Director of the Center for Spatial Information Science and Systems (CSISS), University Research Center, George Mason University. He is also a Professor with the Department of Geography and Geoinformation Science, George Mason University, Fairfax, VA, USA. He has engaged in geoinformation science research for more than 30 years and has published more than 400 publications. He has received as the principal investigator (PI) more than $57 million research grants from U.S. federal agencies and international organizations. His current research activities are mainly in the following areas: geospatial information standards, geospatial cyberinfrastructure, web-based geospatial information and knowledge systems, and geoinformation science applications, particularly in agriculture. From 2010 to 2016, he was the Xhair of INCITS/L1, the U.S. national committee responsible for setting U.S. national standards on geographic information and representing the U.S. at ISO Technical Committee 211 (ISO TC 211). He also was the Elected Chair of Data Archive and Distribution Technical Committee (which has been renamed to Earth Science Informatics Technical Committee) of IEEE Geoscience and Remote Sensing Society from 2005-2009.

Dr. Di has was the recipient of the prestigious awards, such as Merit Award from InterNational Committee on Information Technology Standards, Honor Award from the Secretary of U. S. Department of Agriculture, and R&D Award from the R&D Magazine.